Two-dimensional topological photonics

Alexander B. Khanikaev[1,2]* and Gennady Shvets[3]*

Originating from the studies of two-dimensional condensed-matter states, the concept of topological order has recently been expanded to other fields of physics and engineering, particularly optics and photonics. Topological photonic structures have already overturned some of the traditional views on wave propagation and manipulation. The application of topological concepts to guided wave propagation has enabled novel photonic devices, such as reflection-free sharply bent waveguides, robust delay lines, spin-polarized switches and non-reciprocal devices. Discrete degrees of freedom, widely used in condensed-matter physics, such as spin and valley, are now entering the realm of photonics. In this Review, we summarize the latest advances in this highly dynamic field, with special emphasis on the experimental work on two-dimensional photonic topological structures.

Topology is a branch of mathematics that deals with highly robust conserved quantities that do not change when physical objects are continuously deformed, no matter how much. For example, the number of holes (or handles) of a complex connected surface can be characterized by its genus. This topological index does not change as the surface is deformed without introducing any cuts. Therefore, it can be thought of as being topologically robust. It is not surprising that topology finds a welcoming home in physics, which has a rich tradition (going back to Emmy Noether's theorem) of appealing to conserved quantities such as energy, momentum, angular momentum and many others. It is easy to see, however, how topological indices are more robust than, for example, angular momentum: the class of deformations that preserve topological indices is much broader than that preserving angular momentum. For example, the stringent condition for the conservation of the angular momentum is that the system remains rotationally invariant.

The sea change occurred in the 1980s, when it was realized[1,2] that topological invariants can be introduced for single-particle electron states of a two-dimensional electron gas (2DEG) in a combined periodic potential and out-of-plane magnetic field. These integer topological indices (known as Chern numbers) originate from the quantum nature of the electrons, specifically from their wave-like behaviour in the periodic potential of the lattice. The electron's propagation through the lattice is described by its wavefunction $\psi(\mathbf{x};\mathbf{p})$, where $\mathbf{x}$ is the real-space coordinate and $\mathbf{p}$ is the Bloch quasi-momentum in a periodic lattice. As the Bloch wavenumber is adiabatically changed within the Brillouin zone of the crystalline lattice, its wavefunction acquires a geometrical phase[3] γ (also known as the Berry phase) that cannot be uniquely defined as a function of $\mathbf{x}$ and $\mathbf{p}$ in the topologically non-trivial propagation bands. Therefore, a set of quantities, the Berry connection $\mathscr{A}$ (the gradient of γ) and the Berry curvature Ω (the momentum-space curl of $\mathscr{A}$), which are, respectively, the reciprocal-space equivalents of the vector potential and magnetic field, can be defined (Box 1).

The Chern number can then be introduced as a quantized (that is, integer) flux of the Berry curvature through the Brillouin zone; it characterizes the phase accumulation of the geometrical wave γ as the Bloch wavenumber makes a full circle around the Brillouin zone. While such accumulation of what is commonly known as the Berry phase[3] can occur even in one dimension[4], the most common and widely studied physical systems are two dimensional. Thus, the key feature of all continuous topological

phases is that their topological indices are related to the behaviour of the wavefunctions in the reciprocal space. And, even though an external magnetic field is sufficient for producing non-trivial topological phases in a 2DEG, it was quickly discovered that it is not necessary.

Other types of interaction[2,5,6], such as spin–orbit coupling, can also give rise to topological phases separated by an insulating bandgap. The conservation of another discrete degree of freedom, the valley, was also recently shown[7,8] to produce yet another type of a topological phase, which is responsible for the emerging field of valleytronics[9–11]. But regardless of the nature and dimensionality of topological phases, they share a remarkable property: the emergence of robust bandgap-spanning edge states that exist at the domain wall separating two distinct topological phases (one of which could be a vacuum) that are characterized by different Chern numbers. In condensed-matter physics, the existence of such robust edge states is responsible for a wide range of exotic phenomena, such as the quantum Hall effects, spin-polarized[12] and valley-polarized[10] currents, and many others. The resulting topological systems have the unique property of being insulating in the bulk and conducting at their interfaces owing to presence of chiral one-way or helical spin-polarized edge states. What makes these states particularly interesting is their topologically protected robustness to the presence of a wide class of impurities and defects.

It should not be surprising that many of the quantum topological effects found in condensed-matter systems should find their analogues in photonics. After all, light is a wave, and the above-mentioned topological effects are merely the consequence of the wave nature of the electrons. In the past, photonic crystals have even been referred to as 'semiconductors of light'[13] because some of the best-known features of semiconductors, such as the band structure in the electrons' momentum space that consists of propagation bands separated by bandgaps, are readily replicated with photons. Although photons cannot experience electric potential because they do not carry an electric charge, their motion is governed by the gradients of the refractive index, which plays the role of effective potential (Box 1, left panel).

Nevertheless, emulating many of the key condensed-matter manifestations of topological physics with photons, for example, the quantization of the Hall conductance, is not straightforward because of the key differences between electrons and photons. For example, photons do not possess a half-integer spin of electrons, cannot directly interact with magnetic fields and are not subject
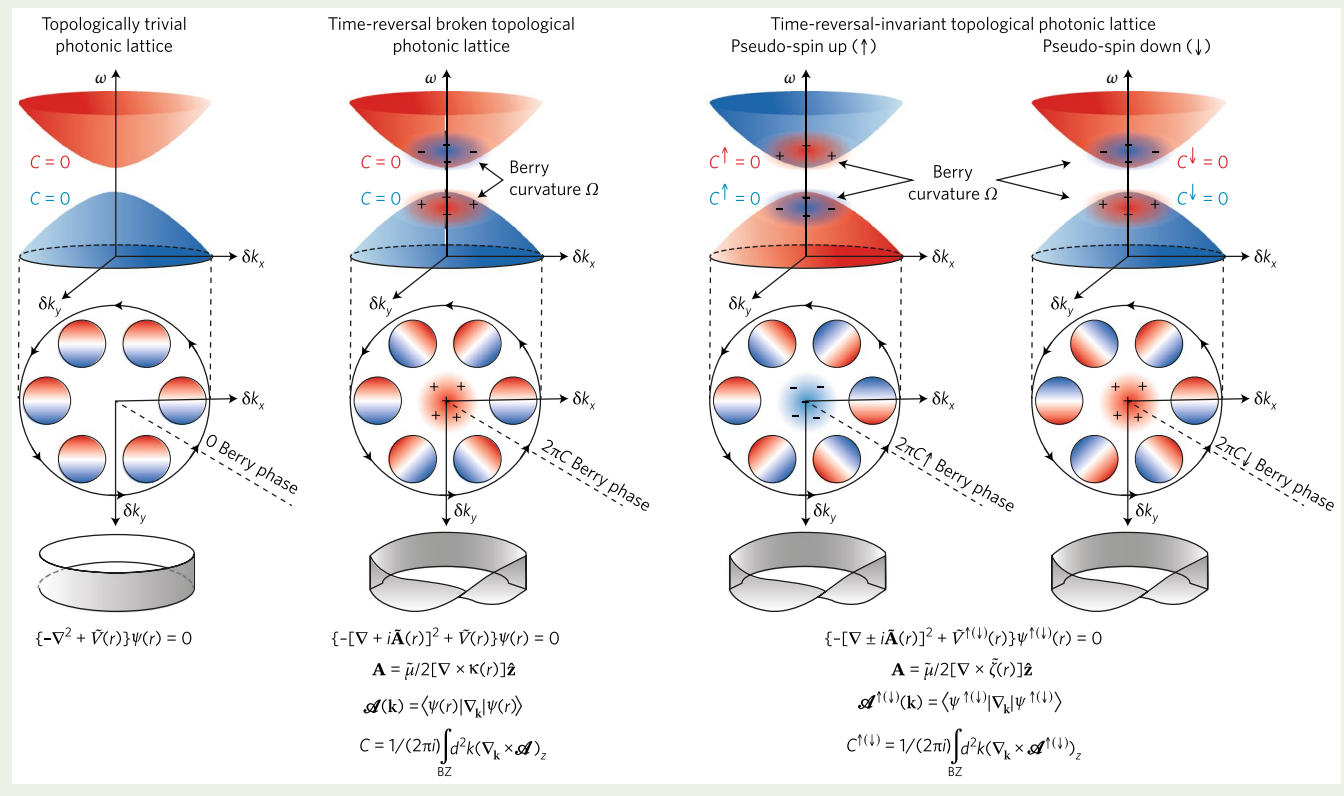
[1]Department of Electrical Engineering, Grove School of Engineering, The City College of the City University of New York, New York, NY, USA. [2]Graduate Center of the City University of New York, New York, NY, USA. [3]School of Applied and Engineering Physics, Cornell University, Ithaca, New York, USA. *e-mail: akhanikaev@ccny.cuny.edu; gshvets@cornell.edu

763

Box 1 | Trivial and non-trivial photonic topological insulators

A topologically trivial photonic crystal is described by a standard wave equation with effective periodic photonic potential $\tilde{V}(r)$ and is characterized by a band structure that consists of isolated bands separated by trivial gaps opened by Bragg diffraction. As illustrated in the left panel, the bands are characterized by a well-defined modal profile, which remains unchanged (up to the Bloch phase factor) over the entire Brillouin zone (BZ). The colour coding applied here is such that the bands with a modal profile characterized by certain symmetry are indicated by the same colour. In topological systems with broken time-reversal symmetry, the magnetization or temporal modulation results in an additional gauge-field contribution $\mathscr{A}(r)$ to the wave equation. The gauge field causes crossing and mixing of the previously degenerate or isolated bands, as indicated by the admixture of an 'alien' colour to the band, and the emergence

of an additional Berry phase contribution to the wavefunction across the Brillouin zone, which has opposite sign (indicated by $\pm$) for two mixing bands. In the example shown in the middle panel, the gauge field results in a non-vanishing Berry connection $\mathscr{A}$ and Berry curvature $\Omega(\mathbf{k})$. An additional Berry phase $\phi_B = \oint \mathscr{A}(\mathbf{k})d\mathbf{l}$ contribution arises as we go around the band-crossing region in the k-space. A similar situation occurs for the case of time-reversal-invariant topological systems, with the difference that the Berry phase appears in two time-reversal partner domains referenced as pseudospin up ↑ and pseudospin down ↓, respectively. In both time-reversal broken and time-reversal-invariant cases, such an extra phase leads to a unique evolution of the field profiles and it cannot be removed by any gauge transformation. (ω is frequency, $\tilde{\eta}$ is the bianisotropy parameter and $\hat{\mathbf{z}}$ is a unit vector in the z direction.)

$$\{-\nabla^2 + \tilde{V}(r)\}\psi(r) = 0$$

$$\{-[\nabla + i\bar{\mathbf{A}}(r)]^2 + \tilde{V}(r)\}\psi(r) = 0$$
$$\mathbf{A} = \bar{\mu}/2[\nabla \times \kappa(r)]\hat{\mathbf{z}}$$
$$\mathscr{A}(\mathbf{k}) = \langle\psi(r)|\nabla_k|\psi(r)\rangle$$
$$C = 1/(2\pi i)\int_{BZ}d^2k(\nabla_k \times \mathscr{A})_z$$

$$\{-[\nabla \pm i\bar{\mathbf{A}}(r)]^2 + \tilde{V}^{\uparrow(\downarrow)}(r)\}\psi^{\uparrow(\downarrow)}(r) = 0$$
$$\mathbf{A} = \bar{\mu}/2[\nabla \times \tilde{\zeta}(r)]\hat{\mathbf{z}}$$
$$\mathscr{A}^{\uparrow(\downarrow)}(\mathbf{k}) = \langle\psi^{\uparrow(\downarrow)}|\nabla_k|\psi^{\uparrow(\downarrow)}\rangle$$
$$C^{\uparrow(\downarrow)} = 1/(2\pi i)\int_{BZ}d^2k(\nabla_k \times \mathscr{A}^{\uparrow(\downarrow)})_z$$

to Fermi statistics. Because of these key differences between electronic and photonic topological phases, the latter must be obtained through judicious photonic designs. This Review provides a concise exposition of some of these design approaches, with special emphasis on experimentally realized 2D photonic structures and the benefits of such designs to the field of photonics. Many experimental and theoretical developments have emerged since the last review of topological photonics[14], making this Review timely for this rapidly evolving field.

The organization of the rest of the Review is schematically represented by Fig. 1, which illustrates the classification map of different approaches to engineering photonic topological states (at the time of writing). The three classes of topological systems depicted in Fig. 1 are: (1) photonic topological insulators (PTIs) with broken time-reversal symmetry; (2) time-reversal invariant PTIs that rely on internal symmetries of the electromagnetic field or on spatial symmetries of the structure; and (3) Floquet PTIs that are periodically modulated in time and/or space. These different categories of

photonic topological states partially overlap due to underlying similarities between different topological phases. All these approaches have been successfully realized in experiments over the past decade.

PTIs with broken time-reversal symmetry

In a natural parallel with the first discovered insulating topological phase of magnetized electrons, the quantum Hall photonic topological insulator (QH-PTI) was the first to be theoretically described[15,16] and experimentally implemented[17]. The implemented 2D photonic structure was designed to operate at microwave frequencies, and comprised a gyromagnetic material embedded in a magnetic field that breaks the time-reversal symmetry. The structure supports photonic topological phases that are mathematically equivalent to the quantum Hall phase of a magnetized 2DEG (Fig. 1), with all its requisite features, such as topological bandgaps and one-way topologically protected edge states that propagate around obstacles without reflection, as shown in Fig. 2a,b and in Box 2. Magnetic photonic crystals have been used as a research
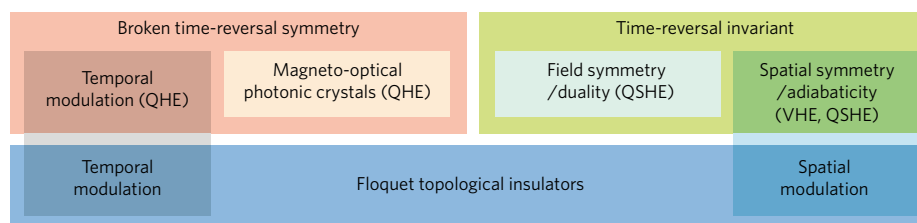
Fig. 1 | Classification scheme of topological orders in 2D photonic systems. The three major classes of photonic topological phases are based on (1) breaking the time-reversal symmetry, (2) conservation of synthetic discrete degrees of freedom based on symmetry or adiabaticity (for example, directional coupling), and (3) spatial or temporal modulation. These three classes, correspondingly, emulate the quantum Hall effect (QHE), quantum spin- and valley-Hall effects (QSHE and QVHE), and the Floquet effect in condensed-matter systems.
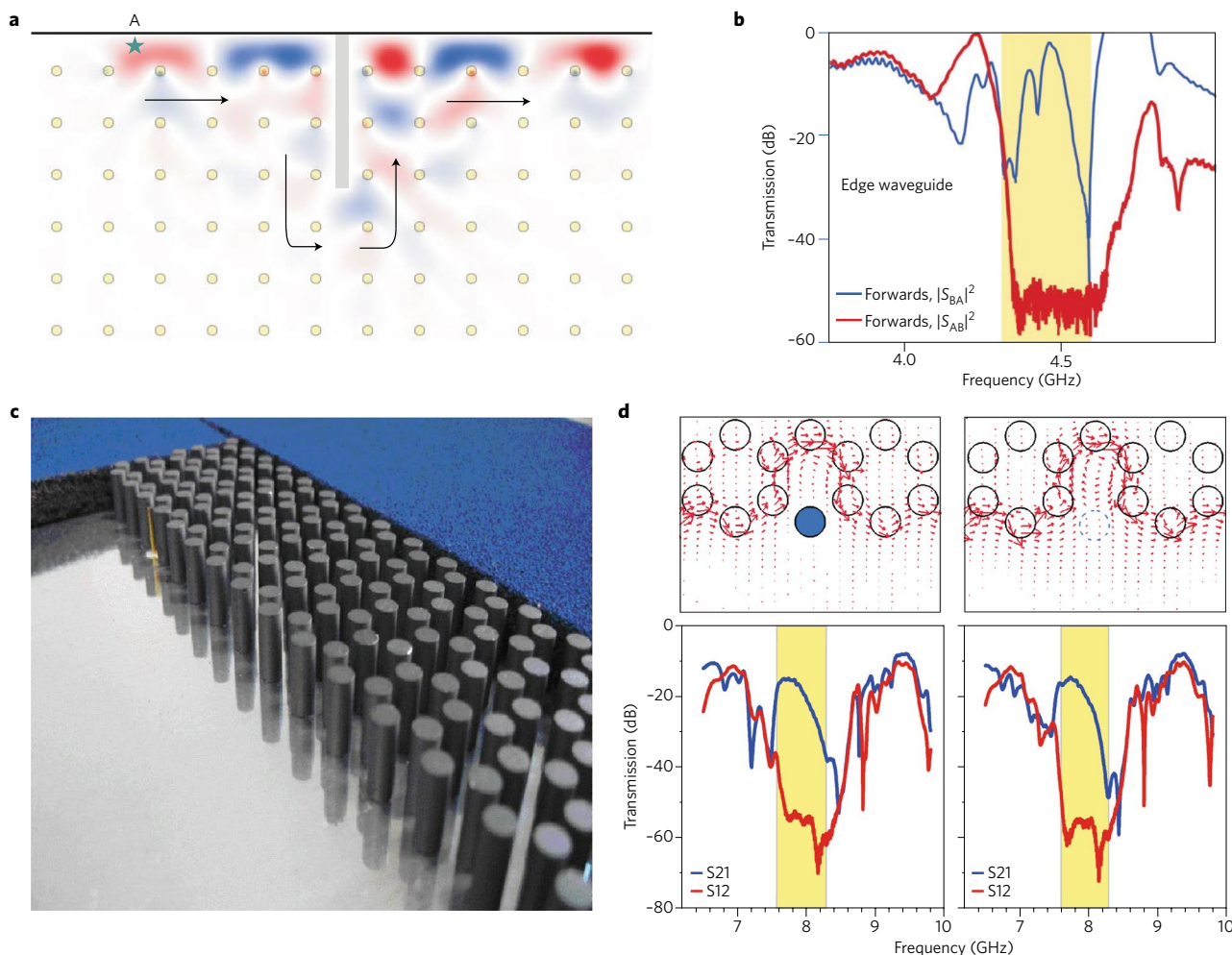
Fig. 2 | Topologically protected photonic transport with broken time-reversal symmetry. a, Robust guiding around perfectly conducting defect shown by the grey region (theoretical calculations). The red and blue show the out-of-plane component of the electric field E_z. The yellow circles show the position of the ferrite rods and the blue star indicates source position. **b**, Experimental observation of the one-way transmission through the topological edge state in the realization of the system shown in **a**. S_{AB} and S_{BA} are transmission from port A to port B and from port B to port A, respectively, and the yellow region indicates the frequency region of the bandgap. **c**, Cladding-free realization of topologically robust transport in photonic graphene. **d**, Theoretical (top) and experimental (bottom) demonstrations of robust transport around defects: metallic rod (filled blue circle) replacing ferrite post (black circles; left) and missing ferrite post (dashed blue circle; right). S12 and S21 are transmission from port 1 to port 2 and from port 2 to port 1, respectively, and the yellow region indicates the spectral position of the topological bandgap. Panels reproduced from: **a,b**, ref. [17], Macmillan Publishers Ltd; **c**, ref. [18], APS. Panel **d** adapted from ref. [18], APS.

platform to explore a variety of topological phenomena, such as cladding-free guiding of topologically protected edge states in photonic graphene lattices[18], steering of multiple edge states along domain walls with large Chern numbers[19,20] and 3D symmetry-protected photon transport[21].

While photons cannot directly experience magnetic fields, it has been shown[16] that finite off-diagonal elements of the magnetic permeability tensor $\mu_{xy} = -\mu_{xy} = i\kappa$ give rise to the effective vector potential (gauge field) $\mathbf{A} \propto e\hat{z} \times \nabla\kappa$ experienced by a photon (Box 1, middle panel). As it turns out, of even greater fundamental

importance is the gradient of the Berry phase $\mathscr{A}(\mathbf{k})$ (also known as the Berry connection), which plays the role of the vector potential in the momentum space. Under the influence of the so-called Berry curvature $\Omega = \nabla_{\mathbf{k}} \times \mathscr{A}(\mathbf{k})$, photonic wave packets propagate in real space as if influenced by the momentum–space analogue of a magnetic field[22].

While it is straightforward to assign the effective real-space vector potential to photons in a gyromagnetic (or gyro-electric[21]) crystal, such assignment is not possible for other types of topological structure, for example, ones that emulate the valley-Hall effect[23]. In such structures, the Berry connection and curvature become essential to describing the photons' topological properties. In fact, the standard classification of 2D topological structures is based on the calculation of their Chern numbers, which are directly connected to the integral over the Berry curvature (Box 1). One of the key properties of a QH-PTI is that it supports one or more one-way edge states at the interface with a topologically trivial medium, such as a perfectly conducting wall (see Fig. 2a,b) or an unpatterned vacuum region (Fig. 2c,d). According to the bulk–boundary correspondence principle[24–26] that was originally formulated for electronic systems, the number of the edge[19,20] states is equal to the bulk Chern number.

Despite the conceptual simplicity of robustness of QH-PTIs, the ability to emulate magnetic fields without using gyromagnetic or magneto-optical materials becomes increasingly important for topological photonic structures operating at optical frequencies. The reason for that is that a large magneto-optical response, which is required for opening a spectrally broad topological bandgap, can only be found in ferrites at microwave frequencies. And even at microwave frequencies, the gyromagnetic approach is not practical because of the large size of the required magnets and absorption in ferrites. Therefore, alternative approaches to producing synthetic gauge fields[27,28] that would result in finite Berry curvature without using a magnetic field are actively pursued, as discussed below. In a broader context, there has been recently a broad range of activities aimed at emulating condensed-matter effects in photonics in a variety of systems. Just to name a few, a synthetic magnetic field was generated and pseudo-Landau levels demonstrated in a multimode ring resonator with a non-planar geometry[29], and spin–orbit coupling for photons and polaritons have been engineered in semiconductor micropillars[30]. These, and other novel photonic platforms, are likely to be used in future topological systems.

Time-reversal invariant photonic topological phases

It has been known for some time that breaking the time-reversal symmetry is not the only way of creating electronic topological phases. As mentioned in the introduction, neither the quantum spin-Hall nor the valley-Hall topological phases require time-reversal symmetry breaking. In fact, it is the time-reversal symmetry that ensures the topological stability of edge states supported by spin-Hall topological insulators[31] in the absence of spin-flipping processes (Box 2, right panel). Other recent developments in condensed-matter physics, such as the discovery of topological orders protected by the lattice symmetry (that is, the crystalline topological insulators[32]) and time-dependent Floquet topological insulators[33], catalysed the development of similar concepts in photonics. However, one should keep in mind that while time-reversal symmetry alone is sufficient to guarantee the presence of degenerate spin-½ states in condensed-matter physics, owing to Kramer's theorem for fermions, this is not the case for photons. Therefore, as we illustrate throughout this Review, additional symmetries are exploited in photonics to achieve time-reversal-invariant topological order.

The earliest proposed time-reversal-invariant photonic topological concept utilized a non-periodic array of coupled silicon ring resonators whose diameters are much larger than the wavelength of light[28,34]. The conserved spin degree of freedom is emulated by the rotation direction of light in the rings, which is preserved by the directional coupling between the rings, and the synthetic vector potential (the synthetic gauge field) is emulated by spatially dependent lengths of the links between the rings.

The idea of engineering a photonic pseudospin degree of freedom by having two degenerate modes connected by time-reversal symmetry[27,28], the condition referred to as spin degeneracy[35], represents one of the cornerstones of topological photonics with preserved time-reversal symmetry. For many recently proposed platforms, such as silicon[28,34] or structured metallic[36] rings, the pseudospins are represented by clockwise and anticlockwise modes. The fundamental reason for this separation of pseudospins is that the total topological Chern number of any time-reversal symmetric photonic structure vanishes. However, separate spin Chern numbers can be assigned to each of the pseudospins[35,37], thus removing the need for time-reversal symmetry-breaking magnetic fields (Box 1).

In the particular case of ring-resonator topological structures[28,34,36], the conservation of pseudospins is the consequence of directional coupling between the rings. However, this is done at the expense of large curvature radii of the ring resonators, thus imposing severe limitations on the footprint of such systems. The need for making the unit cells of topological structures smaller or on the order of the wavelength necessitates a complementary approach to decoupling of pseudospins: designer symmetry protection against spins mixing. The resulting symmetry-protected topological phases represent a broad class of photonic topological systems that do not require breaking time-reversal symmetry, yet enable a wavelength-scale footprint. Such symmetry-protected topological phases can be subdivided into two subclasses according to the symmetries used to engineer the topological state, which can be either (1) an internal symmetry of the field inside the structure or (2) a crystalline symmetry of the lattice. The symmetry can be exploited to produce modal degeneracies in the spectrum that can emulate the spin degree of freedom, thus enabling photonic analogues of the quantum spin-Hall (QSH) effect.

One of the earliest conceptual examples of such a system[35] is a 2D spin-degenerate metacrystal with hexagonal symmetry comprising metamaterials-based unit cells with equal electric permittivity and magnetic permeability tensors, $\widehat{\epsilon}$ and $\widehat{\mu}$, respectively. The $\widehat{\epsilon} = \widehat{\mu}$ condition, which can be approximately satisfied in a finite frequency range in electromagnetic metamaterials, enables one to construct degenerate spin states out of the linear combinations of transverse electric and transverse magnetic waves. A synthetic gauge field acting separately and unequally on the two spin states could be then engineered through additional metamaterials design, so that the two spin states experience opposite effective Berry curvatures. It has been theoretically shown[35] that such a gauge field can be generated by breaking the inversion symmetry in the vertical direction and inducing a bianisotropic (also known as the high-frequency magneto-electric) coupling between the transverse electric and transverse magnetic modes (Box 1). Specifically, the bianisotropic response is described by the constitutive relations that relate the electric displacement field {$\mathbf{D}$} and magnetic field {$\mathbf{B}$} to the electric field {$\mathbf{E}$} and magnetic intensity {$\mathbf{H}$} according to: $\mathbf{D} = \widehat{\epsilon}\mathbf{E} + \widehat{\chi}\mathbf{H}$ and $\mathbf{B} = \widehat{\mu}\mathbf{H} + \widehat{\chi}^{+}\mathbf{E}$, where $\widehat{\chi}$ is the magneto-electric parameter with the following non-vanishing components: $\chi_{xy} = -\chi_{xy} = i\zeta$, where ζ is the strength of magneto-electric coupling. Just as the off-diagonal components of the magnetic permeability tensor give rise to the effective gauge field $\mathbf{A}$ and the Berry connection $\mathscr{A}(\mathbf{k})$ in QH-PTIs, so does the above bianisotropy separately produce the gauge field and the Berry connection for each of the two spin components, giving rise to a QSH-PTI, as explained in Box 1.

The concept of bianisotropy-induced QSH-PTIs was successfully realized in many experiments[37–41] that demonstrated the existence and topological protection of the edge states. The robustness of such topologically protected edge waves (TPEWs) against bending of
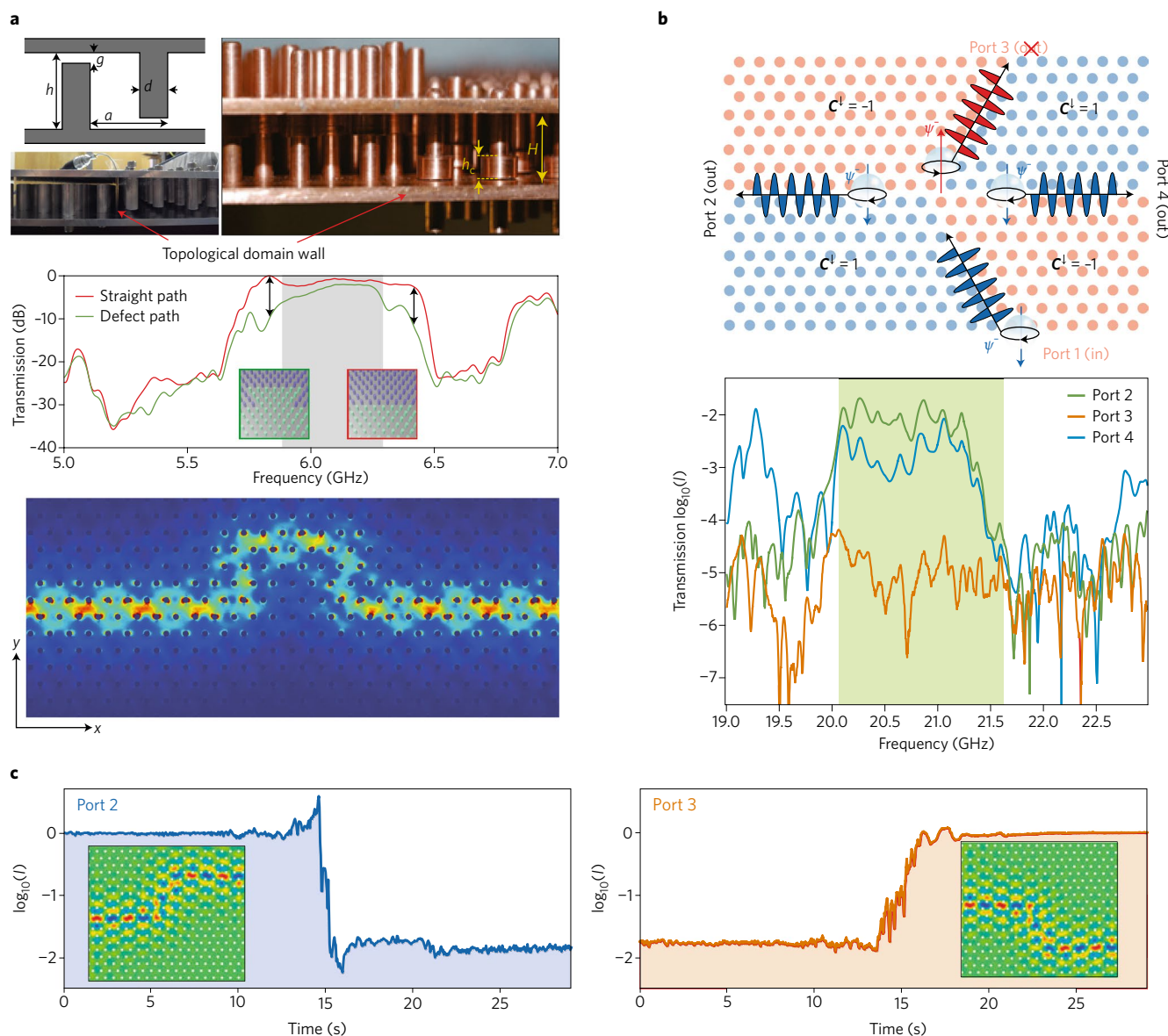
Fig. 3 | Topological photonics in meta-waveguides with bianisotropy-induced spin–orbit interactions. a, Top: examples of topological meta-waveguides. h and H are the distance between parallel plates of waveguides, g is the gap size, d is the diameter of rods, h_c is height of the collar, and a is a lattice constant. Middle and bottom: robust guiding around sharp corners. The insets in the middle panel show the path of an electromagnetic wave along the reconfigurable domain wall. The bottom panel shows time-resolved transmission through a reconfigurable domain wall. **b**, Spin-polarized wave-division at a topological four-port junction. The green region indicates the spectral position of the topological bandgap. **c**, Robust steering of an electromagnetic wave using reconfigurable synthetic gauge field produced by bianisotropy. I, intensity of transmitted signal. Panels reproduced from: **a**, top right, ref. [38], Macmillan Publishers Ltd, top left, middle and bottom, top right, ref. [39], under a Creative Commons licence (https://creativecommons.org/licenses/by/4.0/); **b,c**, ref. [38], Macmillan Publishers Ltd.

the domain wall and symmetry preserving disorder[38]. This robustness manifests as the reflectionless propagation of electromagnetic radiation around sharp corners, as illustrated in Fig. 3a, and across disordered regions. Active topology control through reconfigurable gauge fields was also demonstrated using mechanical movements of the constituent elements of the PTIs, thus enabling wave steering, as shown in Fig. 3c. Among other important advantages brought up by the topology are also the possibility to build topological delay lines where the wave can acquire an arbitrary phase without the need of coupling to resonances[24], and spin-polarized wave division at topological multiport junctions, as shown in Fig. 3b[23]. The chiral nature of the TPEWs[42], that is, the possibility of launching directional edge states using a circularly polarized emitter, has also been experimentally demonstrated[39].

To better illustrate the differences and similarities between using QH-PTIs and QSH-PTIs for topologically protected wave propagation, we focus on one of the simplest realizations based on a metallic parallel plate waveguide with an embedded triangular array of metal rods[42], shown in Fig. 3a. The geometrical parameters of this vertically confining 2D structure can be engineered to produce a doubly degenerate spectrum with two pairs of overlaid Dirac cones each corresponding to transverse electric and transverse magnetic polarized modes, thus enabling spin emulation. As the next step, the bianisotropic response emulating the spin–orbit coupling can be introduced by exploiting the different symmetries of transverse electric and transverse magnetic modes with respect to the inversion symmetry in the vertical direction. It was theoretically proposed[42] that the topological bandgap can be produced either by

Box 2 | Topologically robust transport of chiral and helical edge states

The topologically non-trivial properties of the bulk give rise to the emergence of a new class of electromagnetic states spectrally located within the range of the topological bandgap and crossing it interconnecting upper and lower bands. These states are confined to the boundaries of the system and are referred to as topological edge states. According to the bulk–boundary correspondence principle, the number of such edge states on a particular interface is determined by the difference in the band Chern numbers across the interface calculated for a particular frequency ω_0 within the bandgap, where the band Chern number is defined as the sum of all Chern numbers of the bands below this frequency $C^B = \sum_{n(\omega_n < \omega_0)} C^n$, where n is the band number. The panels illustrate three possible scenarios for 2D systems. The left panel shows the case of an interface between two topologically trivial structures ($C^B = 0$) in both domains, which can host only conventional (non-topological) surface states whose dispersion is itself gapped within the (topologically trivial) bandgap of 2D bulk bands projected onto the 1D interface. In the case of a topological system with broken time-reversal symmetry shown in the middle panel,

the projected 2D band structure shows a non-trivial topological bandgap with the edge modes crossing the entire bandgap. Such modes are non-reciprocal and can carry energy only in one direction along the domain wall. Owing to such unidirectionality, these guided modes are referred to as one-way (or chiral) edge states. The lack of solution that would carry energy in the reverse direction leads to complete suppression of backscattering, which endows the topological edge states with robustness against defects and disorder (middle panel). In the case of symmetry-protected topological order with time-reversal symmetry, the spin-up and spin-down domains both possess similar unidirectional topological edge states (right panel). Similar to the bulk states, the edge states of two domains appear to be time-reversal partners transforming one into another under the inversion of the arrow of time. Despite the fact that the partner can always carry energy in the opposite direction, the backscattering appears to be still suppressed as long as defects and disorder do not mix spins and the edge states, referred to as spin-polarized one-way (or helical) edge states, exhibit topological robustness.
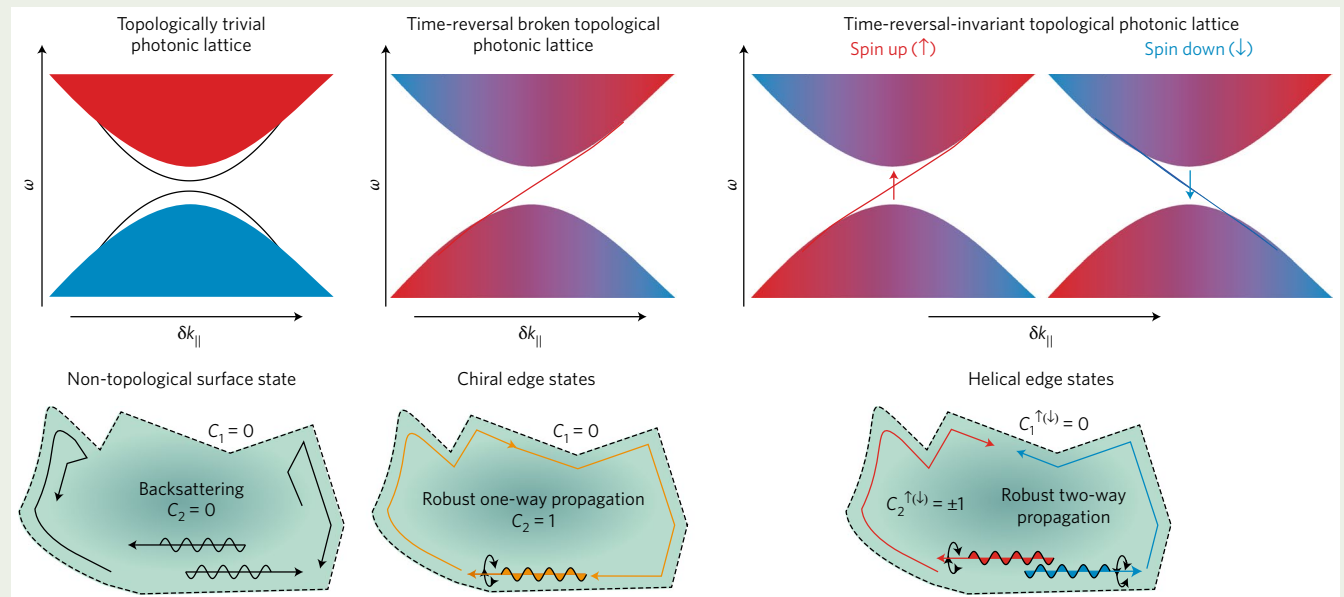
introducing air gaps between the rods and just one of the parallel plates or by adding a wider section to the rods. Both experimental approaches[38,39] (Fig. 3a) rely on bianisotropic coupling between the transverse electric and transverse magnetic modes, preserve the spin-degeneracy, and emulate the spin–orbit interactions of the Kane-Mele type that were originally used to describe the quantum spin-Hall effect in graphene[5].

Although the total Chern number, as calculated by summing up over all modes and integrating over the Brillouin zone, is zero (unlike in the case of QH-PTIs), each of the spin states is topologically non-trivial, and is characterized by the spin-Chern numbers $C_{\uparrow\downarrow} = \pm sign(\Delta_{SOM})$, where Δ_{SOM} is proportional to the topological bandgap induced by the bianisotropy. The sign of Δ_{SOM} determines the order of the bands at the high-symmetry corners of the Brillouin zone (K and K′), and is defined by the nature of the bianisotropic asymmetry (for example, whether the air gap is at the top or bottom plates). The latter property enables topological interfaces ('domain walls') between PTIs with opposite signs of Δ_{SOM} and, therefore, between photonic topological phases with opposite spin-Chern

numbers. It has been known in condensed-matter physics for such domain walls separating topologically non-trivial electron phases with different Berry curvatures to support multiple bandgap-crossing edge states[24–26]. In the photonics context, such chiral states that exhibit spin-locked propagation are referred to as TPEWs.

There are several key differences between the edge states that exist at the domain walls of QH-PTIs and QSH-PTIs. First, the TPEWs at the edge of QH-PTIs are strictly non-reciprocal, that is, support only one-way propagation. In contrast, the TPEW at the edges and the domain walls of QSH-PTIs are spin-polarized, but reciprocal, that is, they propagate in the direction locked to their spin. Therefore, in the case of QSH-PTIs, each spin-polarized edge state $\psi^{\uparrow}(k_{\parallel})$ has an opposite spin $\psi^{\downarrow}(-k_{\parallel})$ propagating in the opposite direction. As expected for the system with time-reversal symmetry, these states are connected by the time-reversal operation. As a consequence, violations of the symmetry responsible for the emergence of the pseudospin, as well as the time-reversal breaking, couple such states, effectively destroying their topological protection.
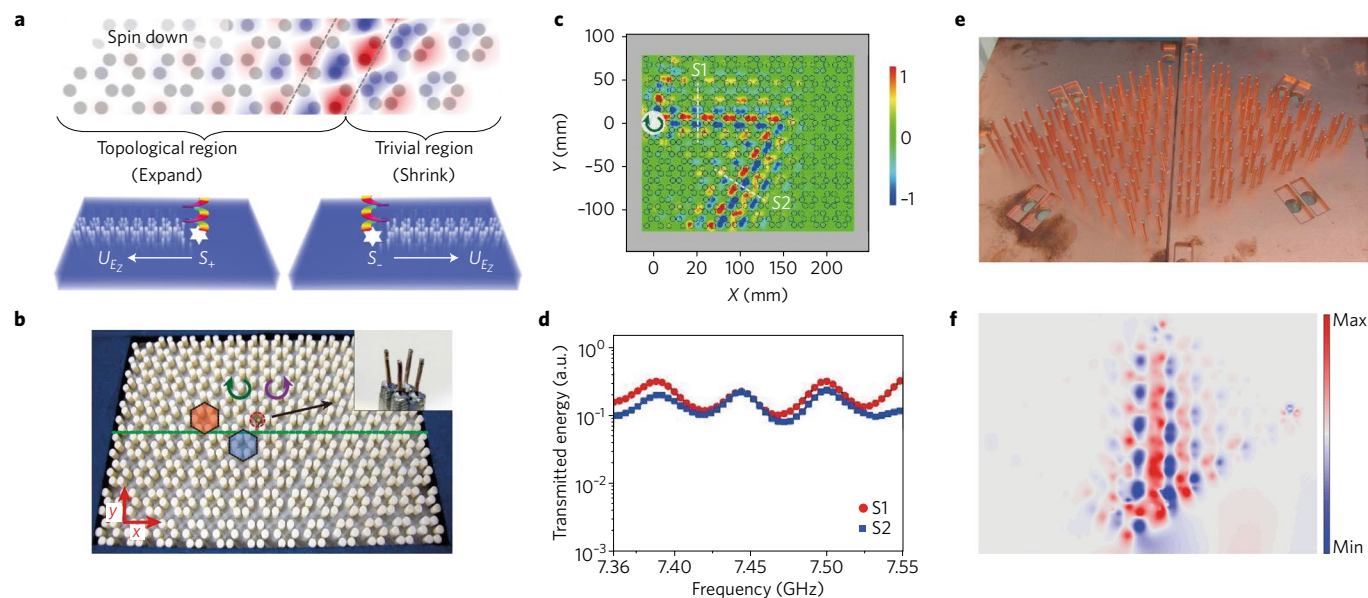
Fig. 4 | Photonic topological insulator protected by lattice symmetry. a, 2D geometry and field distribution of the edge state confined to the domain wall between trivial and non-trivial regions obtained by shrinkage (right) and expansion (left) of the dielectric hexamer constituting the unit cell of the crystal. S_+ and S_- are circularly left and circularly right polarized sources, respectively, and U_{E_z} is the Poynting vector. **b**, Experimental microwave realization of the all-dielectric structure with source (enlarged region) placed in the centre of the domain wall (green horizontal line). The coloured arrows indicate the handedness of the field and the hexagons show distorted unit cells across the domain wall. **c,d**, Guiding of the edge state by a sharply bent domain wall: 2D map of measured field profile (**c**) and transmission spectrum (**d**). S1 and S2 in d show the field intensity measured at corresponding locations in c. **e**, Metal antenna array implementing analogous topological crystalline order on the subwavelength scale. The structure shown possesses a domain wall between the shrunk and expanded regions. **f**, Experimentally mapped near-field of an edge state guided by the domain wall. Panels adapted from: **a**, ref. [43], APS; **f**; ref. [60], Macmillan Publishers Ltd. Panels reproduced from: **b–d**, ref. [59]; **e**, ref. [60], Macmillan Publishers Ltd.

The edge states in the QH-PTI case have been observed either at the interface between the topological non-trivial and topologically trivial (metal wall[17] or air[18]) domains, or between two topologically non-trivial domains[20]. Similarly, topologically protected edge states have been experimentally observed at the edge of a QSH-PTI and free space for the system based on directionally coupled ring resonators[34,36]. The edge states at a domain wall between topologically trivial photonic crystals and QSH-PTIs have also been theoretically predicted[35,43] and experimentally realized[37] in bianisotropic meta-waveguides. Of considerable interest are recent experimental observations[38,39,41] of TPEWs (sometimes referred to as the kink states by analogy with condensed-matter systems[44]) localized at interfaces between two PTIs with opposite values of spin-projected Berry curvature, which allow the propagation of topological edge states to be controlled by dynamically changing the location of the domain walls through switching the sign of synthetic gauge fields. Despite their seemingly fragile nature, edge states in QSH-PTIs have been shown to be robust against a broad range of disorders, including sharp bending and random distribution of the synthetic gauge field[38,39], as well as against lattice disorder[45,46]. Detailed experimental comparisons between topologically trivial and protected guided modes demonstrated that only the latter exhibit broadband reflection-free propagation along sharply bent waveguides[39].

Another concept that is attracting considerable attention in photonics is that of a valley: an additional discrete degree of freedom in photonic crystals with C_{6v} point symmetry. Viewed as a pseudospin degree of freedom, the valley refers to the proximity of one of the two high-symmetry corners $\mathbf{k}_K = (4\pi/3a_0, 0)$ and $\mathbf{k}_{K'} = (-4\pi/3a_0, 0)$ of the Brillouin zone of a hexagonal crystal lattice with lattice constant a_0. The valley degree of freedom recently gained prominence in condensed-matter physics in the context of valleytronics (that is, valley-locked propagation) for a wide variety of materials, including AB–BA stacked electrically biased bilayer graphene[10,11,47], silicene[48] and graphene placed on top of hexagonal boron nitride[49]. Crucially, under a broad set of perturbations[23] that cannot scatter photons from one valley into another, this degree of freedom can be considered to be conserved. There is a growing interest in exploiting the valley degree of freedom in photonics, and designing a new class of quantum valley Hall PTIs (QVH-PTIs)[23,46,50–52]. It has been theoretically demonstrated[23,46] that, in a triangular array of dielectric or metal rods satisfying the C_3 point symmetry, the reduction of the lattice symmetry leads to a non-vanishing Berry curvature of the bands at this point and a topological transition to the valley-Chern state.

Specifically, under the valley-conservation assumption, it becomes appropriate to consider a restricted topological phase of photons that is defined in only one of the two valleys. Such phases are commonly referred to as merons[6,53,54], and are characterized by restricted (valley projected) half-integer Chern numbers associated with their spin and valley: $C_{\uparrow\downarrow}^{(\nu)} = \pm\frac{1}{2}$, where $\nu = K, K'$, and $C_{\uparrow\downarrow}^{(\nu)}$ for each spin state are obtained by integrating the Berry curvature over a restricted region of the Brillouin zone that coincides with one of the valleys. The bulk–boundary correspondence principle prohibits edge states at the interface between a meron topological phase and a topologically trivial phase. However, the edge states at the domain wall between PTIs with half-integer spin-valley Chern numbers of the opposite sign are allowed regardless of whether the two PTIs are of the same type (for example, two QVH-PTIs or QSH-PTIs) or not[46]. In condensed-matter physics, such 1D chiral states are sometimes referred to as valley-Hall kink states[44,55–57] to distinguish them from the more conventional edge states that exist at the periphery of a topological insulator. The conservation of the valley degree of freedom depends on the shape of the domain

wall separating the QVH-PTI from, for example, free space, or from another QVH-PTI: the zigzag-shaped domain walls preserve the valley whereas the armchair-shaped ones do not[23]. Valley conservation enables yet another recently discovered phenomenon: a 'perfect' refraction of the valley-kink states into free space[58].

A different approach to topology relying on the lattice symmetry and the valleys was introduced in ref. [43], where the valley degree of freedom was used as a pseudospin to emulate QSH-PTIs in a photonic system. A synthetic gauge field was emulated using a particular symmetry reduction of the hexagonal lattice of dielectric rods — shrinking or expansion of a group of six nearest Si rods as illustrated in Fig. 4a — the transformation that changes the shape of the unit cell and the Brillouin zone of the lattice, giving rise to the folding of the original lattice valleys into the centre of the Brillouin zone of the new (expanded) lattice. The transformed lattice is triangular, with a unit cell comprising hexamer-shaped photonic 'molecules' supporting hybridized dipolar and quadrupolar circularly polarized eigenmodes. These circularly polarized doubly degenerate states play the role of spin-up ($\uparrow$) and spin-down ($\downarrow$) states, and the synthetic gauge field generated by the rods' expansion leads to band inversion and topologically non-trivial bulk bands below the bandgap that possess integer spin-Chern numbers $C_{\uparrow\downarrow} = \pm 1$. In contrast, the shrinkage of the rods produces a gapped but topologically trivial state ($C_{\uparrow\downarrow} = 0$). The fact that two photonic systems with identical lattice types support either trivial or topological phases at the same frequency makes it a convenient platform for realizing the domain walls and the edge states localized at the walls (Fig. 4b). It has been experimentally confirmed in microwave systems[59,60] for both all-dielectric and metal-based systems (shown in Fig. 4b–d and Fig. 4e,f, respectively) that such crystalline photonic topological systems host edge states, which, however, can become gapped because the interface itself may break the symmetry responsible for the topological order. Nonetheless, as evidenced in Fig. 4c[59], the edge states show a significant degree of protection against sharp bending of the interface, as well as against defects in its proximity[43]. More recently, a similar design was used in the optical domain to control light scattering in silicon-based metasurfaces by tuning a synthetic gauge field[61].

The approach based on symmetry-protected topological order in time-reversal-invariant photonic systems has apparent disadvantages compared with that based on broken time-reversal symmetry. Indeed, engineering symmetries is not straightforward and may require cumbersome designs that may be hard to realize in practice. Moreover, inability to guarantee the presence of such symmetries across the entire structure, including the interfaces (where the edge modes localize), may have a detrimental effect on the topological order and robustness of the edge states[43]. Indeed, the violation of the symmetry affects the photonic edge states in the same way as magnetic defects in electronic systems with topology protected by time-reversal symmetry, leading to the spin-flip of a photonic pseudospin generated by the symmetry. This limitation applies equally to the case of topological photonic orders induced by the duality and by the spatial lattice symmetry, with the difference that the topological interface itself typically does not break duality and the edge states in such systems appear to be gapless. The same is true for the array of ring resonators, where clockwise and anticlockwise modes remain decoupled, and the edge states are gapless both at the domain walls and at the edges. In the case of topological orders protected by the lattice symmetry, structures may require additional optimization to minimize the detrimental effect of symmetry breaking by interfaces and domain walls.

Floquet topological photonic systems

An alternative approach to topology that is free of the limitations of symmetry-protected systems and also does not require magnetization or magnetic materials is based on temporal modulation and was independently introduced in condensed-matter physics[33,62] and photonics[63,64], and, in analogy to its condensed-matter counterpart,

is often referred to as Floquet topological order. In photonics, it has been shown that a non-uniform temporal modulation of the system can generate a synthetic gauge field with an arbitrary spatial distribution, giving rise to a variety of topological effects, including emergence of one-way surface states and modification of the wave-packet dynamics — essentially the Hall effect of light[64]. Unfortunately, this approach requires modulation of dielectric parameters of the photonic system, which should be both sufficiently fast and strong, and therefore is hard to implement in practice. Although the synthetic magnetic field generated by temporal modulation has been experimentally implemented, in particular, to achieve non-reciprocal behaviour without magnetic materials[65–69], topological order of the Floquet class based on temporal modulation has not been experimentally realized.

Despite lacking experimental realization of true topological Floquet systems, this concept has been very fruitful in photonics and was tested in a variety of systems based on arrays of coupled dielectric waveguides with modulation in time emulated with modulation in space. In particular, a photonic crystal comprising a 2D hexagonal array of twisted fibres[70] was recently considered. Under paraxial approximation, this system is described by a Schrödinger-type equation, where the time variable is replaced by the propagation distance along the fibres and the periodic twisting replaces temporal modulation. This fact was evidenced by the emergence of a synthetic magnetic field in the effective wave-equation describing the dynamics of the field amplitude in the system. Experimental results unequivocally confirmed that twisting of the waveguides results in the topological Floquet state, causing opening of photonic bandgaps and the emergence of topological edge states at the open ends of the waveguide array. Robustness of the edge states has also been confirmed by direct observation of their reflectionless propagation across sharp corners between different cuts of the lattice, as well as by the ability of modes to propagate around deliberately introduced defects — missing waveguides.

To avoid coupling between different Floquet orders, the authors considered the case of fast-rotating modulation, which gives rise to the emergence of an effective magnetic field and a topological state characterized by a non-vanishing Chern number. More recently, two groups independently lifted the condition of fast modulation and demonstrated experimentally[71,72] another topological class of so-called anomalous Floquet insulators[73,74], shown in Fig. 5a,b. Despite vanishing Chern numbers, these systems have been shown to host robust edge states, which, however, appear within the bandgaps open due to hybridization of bands corresponding to different Floquet orders.

Interestingly, a rigorous mathematical connection has also been found between the Floquet topological systems and 2D networks and arrays of ring resonators, providing a mechanism for direct mapping and emulation of Floquet states in this platform[74]. In particular, a microwave network has been used to experimentally measure topological edge invariants[75]. In another study[36], a similar mapping was used to emulate anomalous Floquet insulators in an array of ring resonators formed by closely spaced subwavelength metallic rods, shown in Fig. 5c. The near-field coupling between the rods enables transfer of electromagnetic radiation and appearance of collective modes known as 'spoof' or 'designer' plasmons, whose dispersion characteristics can be widely tuned by adjusting dimensions of the rods and their spacing. Such designer photonic modes therefore represent a powerful instrument for engineering topological responses across the entire electromagnetic spectrum, with the first experimental realization in the microwave domain[36] demonstrating edge transport via topological designer plasmons (Fig. 5d). In the same study, the authors systematically investigated robustness of the edge states to defects and showed that they are robust against removal
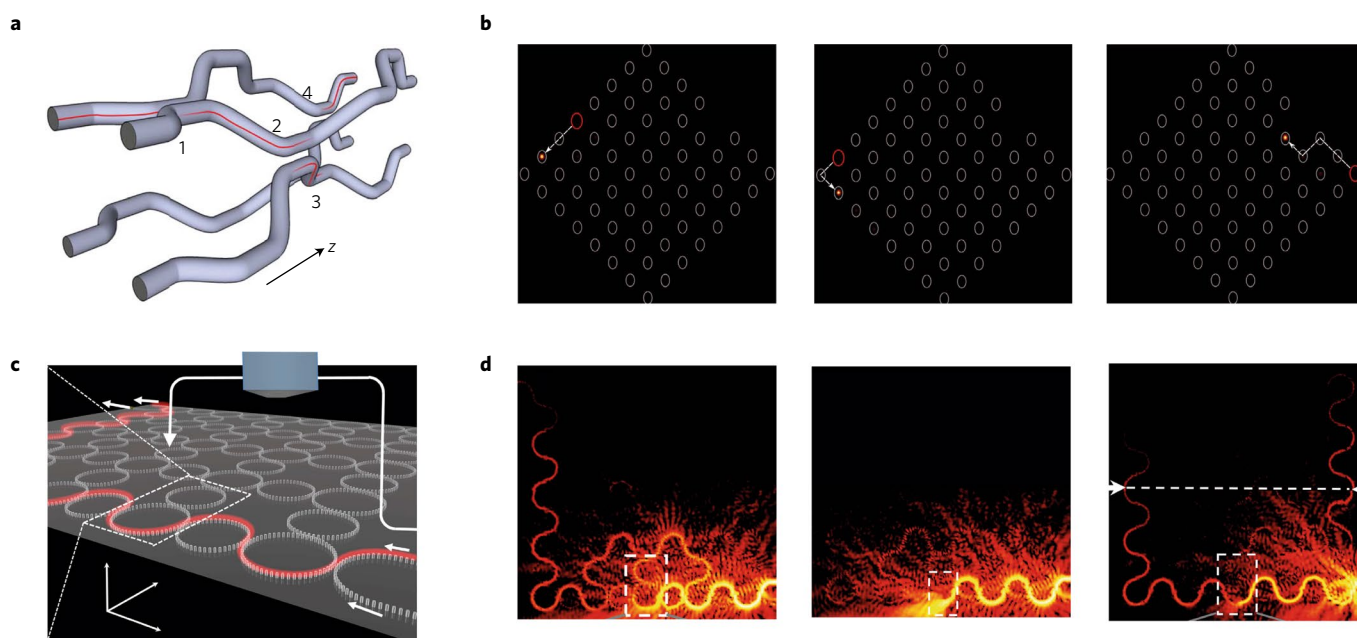
Fig. 5 | Floquet topological insulators with spatial modulation. a, Schematic of anomalous Floquet insulator based on a 2D array of laser-written optical waveguides. The numbers indicate proximal segments of the waveguides where the transfer of the guided mode, schematically shown by red line, takes place. **b**, Topologically robust edge transport induced by the spatial modulation of coupled waveguides shown in **a** in the z direction. **c**, 2D system network of rings supporting spoof plasmons that can be mapped onto a Floquet topological insulator. The small arrows show the direction of energy flow, and the large curved arrow indicates the probe of the near field. The red line indicates the path of the wave in the structure. The blue block is the apparatus that measures the near field from the probe. **d**, Demonstration of robustness against bending (left), and the lack of robustness against dissipative defects (middle) and defects causing flipping of the pseudospin (right). The colour shows the intensity of the guided edge state and the dashed rectangles indicate position of defective cells. Panels reproduced from: **a**, ref. [72], Macmillan Publishers Ltd; **c**, ref. [36], Macmillan Publishers Ltd. Panels adapted from: **b**, ref. [72], Macmillan Publishers Ltd; **d**, ref. [36], Macmillan Publishers Ltd.

of some of the rings from the lattice. The authors also for the first time considered the effect of a dissipative defect and showed that the edge states are not robust to it as well as to imperfections in the rings, causing back reflection of the spoof plasmons, emphasizing the importance of eliminating such defects in Floquet systems emulated with spatial periodicities.

Finally, we note that while the majority of topological photonics research is concerned with the observation of robust edge states because of their importance for applications, one should keep in mind that, according to the bulk–interface correspondence, these edge properties emerge from the topological properties of the photons propagating in the bulk. Therefore, studies of bulk topological properties are interesting on their own. Because topological properties of the bulk states affect their propagation, topological invariants have been directly extracted for 1D[76] and 2D[61] systems. A different approach to extracting a winding number was taken by Mittal et al.[77] who introduced a unit quantum flux at the edge and observed a shift in the position of the edge spectrum.

Conclusions and outlook

While the field of topological photonics is still in its infancy, a large number of successful experimental results have demonstrated its transformative potential for fundamental and applied photonics. While here we focused on 2D systems, which we believe are of the utmost importance for practical applications, there is an outpouring of new experimental results in 1D[78] and 3D[79–81], and even a proposal for the realization of second Chern class topological 4D systems in 3D[82] photonic structures followed by recent implementation in a 2D system of coupled waveguides[83]. Topological quasicrystals is another emerging field, where topology can be created by exploiting even higher dimensions where quasicrystals appear

to be periodic[84,85]. Another groundbreaking generalization of the Floquet topological order using the multi-spectral response of photonic cavities envisions additional synthetic dimensions in the frequency domain, thus implementing 3D topological physics in 2D structures[86].

Of more practical interest are the recent proposals of valley-polarized transport in metamaterials[23,87], especially in the context of combining different types of topological phase into pseudospin filtering junctions[46]. Even more practical revolutionary proposals aim to redefine laser systems by endowing them with topological robustness[88] and quantum-limited travelling wave amplifiers that are protected against both internal losses and backscattering[89].

Looking further ahead, a particularly promising direction in topological photonics is to go beyond the linear regime towards strong photon–photon and photon–matter interactions in topological environments. For example, strong coupling of photons to phonons has been suggested as one approach to generating synthetic gauge field for light in photonic lattices supporting both photonic and phononic modes[90]. Another promising multiphysics platform is based on polaritons, where 'topolaritons', the topological polaritonic excitations whose topological properties emerge from strong light–matter coupling, for example, in 2D quantum systems[91,92]. Recent experimental results[93] for a 2D polaritonic honeycomb lattice demonstrated the presence of polaritonic zero-energy edge states characterized by a 1D topological invariant. Finally, developing a strongly interacting topological photonic platform for studying fractional Hall states of bosons[94–97] is another (albeit distant) promising application of nonlinear topological photonics. While many of the concepts proposed within the field of topological photonics are likely to remain of purely fundamental interest, there is no doubt that the unique properties of photonic topological phases will secure their place in future applications[98,99].

References

1. Thouless, D. J., Kohmoto, M., Nightingale, M. P. & den Nijs, M. Quantized Hall conductance in a two-dimensional periodic potential. *Phys. Rev. Lett.* **49**, 405 (1982).
2. Haldane, F. D. M. Model for a quantum Hall effect without Landau levels: condensed-matter realization of the "parity anomaly". *Phys. Rev. Lett.* **61**, 2015–2018 (1988).
3. Berry, M. V. Quantal phase factors accompanying adiabatic changes. *Proc. R. Soc. Lond. Ser. A* **392**, 45 (1984).
4. Su, W. P., Schrieffer, J. R. & Heeger, A. J. Solitons in polyacetylene. *Phys. Rev. Lett.* **42**, 1698 (1979).
5. Kane, C. L. & Mele, E. J. Quantum spin Hall effect in graphene. *Phys. Rev. Lett.* **95**, 226801 (2005).
6. Bernevig, B. A., Hughes, T. L. & Zhang, S.-C. Quantum spin Hall effect and topological phase transition in HgTe quantum wells. *Science* **314**, 1757–1761 (2006).
7. Rycerz, A., Tworzydło, J. & Beenakker, C. Valley filter and valley valve in graphene. *Nat. Phys.* **3**, 172–175 (2007).
8. Xiao, D., Yao, W. & Niu, Q. Valley-contrasting physics in graphene: magnetic moment and topological transport. *Phys. Rev. Lett.* **99**, 236809 (2007).
9. Yao, W., Xiao, D. & Niu, Q. Valley-dependent optoelectronics from inversion symmetry breaking. *Phys. Rev. B* **77**, 235406 (2008).
10. Ju, L. et al. Topological valley transport at bilayer graphene domain walls. *Nature* **520**, 650–655 (2015).
11. Kim, Y., Choi, K., Ihm, J. & Jin, H. Topological domain walls and quantum valley Hall effects in silicene. *Phys. Rev. B* **89**, 085429 (2014).
12. Moore, J. E. The birth of topological insulators. *Nature* **464**, 194–198 (2010).
13. Yablonovitch, E. Photonic crystals: semiconductors of light. *Sci. Am.* **12**, 47 (2001).
14. Lu, L., Joannopoulos, J. & Soljačić, M. Topological photonics. *Nat. Photon.* **8**, 821–829 (2014).
15. Raghu, S. & Haldane, F. Analogs of quantum-Hall-effect edge states in photonic crystals. *Phys. Rev. A* **78**, 033834 (2008).
16. Wang, Z., Chong, Y., Joannopoulos, J. & Soljačić, M. Reflection-free one-way edge modes in a gyromagnetic photonic crystal. *Phys. Rev. Lett.* **100**, 13905 (2008).
17. Wang, Z., Chong, Y., Joannopoulos, J. D. & Soljačić, M. Observation of unidirectional backscattering-immune topological electromagnetic states. *Nature* **461**, 772–775 (2009).
18. Poo, Y., Wu, R., Lin, Z., Yang, Y. & Chan, C. T. Experimental realization of self-guiding unidirectional electromagnetic edge states. *Phys. Rev. Lett.* **106**, 093903 (2011).
19. Skirlo, S. A., Lu, L. & Soljačić, M. Multimode one-way waveguides of large Chern numbers. *Phys. Rev. Lett.* **113**, 113904 (2014).
20. Skirlo, S. A. et al. Experimental observation of large Chern numbers in photonic crystals. *Phys. Rev. Lett.* **115**, 253901 (2015).
21. Lu, L. et al. Symmetry-protected topological photonic crystal in three dimensions. *Nat. Phys.* **12**, 337 (2016).
22. Xiao, D., Chang, M.-C. & Niu, Q. Berry phase effects on electronic properties. *Rev. Mod. Phys.* **82**, 1959 (2010).
23. Ma, T. & Shvets, G. All-Si valley-Hall photonic topological insulator. *New J. Phys.* **18**, 025012 (2016).
24. Hasan, M. Z. & Kane, C. L. Topological insulators. *Rev. Mod. Phys.* **82**, 3045–3067 (2010).
25. Mong, R. S. & Shivamoggi, V. Edge states and the bulk-boundary correspondence in Dirac Hamiltonians. *Phys. Rev. B* **83**, 125109 (2011).
26. Ezawa, M. Topological Kirchhoff law and bulk-edge correspondence for valley Chern and spin-valley Chern numbers. *Phys. Rev. B* **88**, 161406 (2013).
27. Umucalılar, R. O. & Carusotto, I. Artificial gauge field for photons in coupled cavity arrays. *Phys. Rev. A* **84**, 043804 (2011).
28. Hafezi, M., Demler, E. A., Lukin, M. D. & Taylor, J. M. Robust optical delay lines with topological protection. *Nat. Phys.* **7**, 907–912 (2011).
29. Schine, N., Ryou, A., Gromov, A., Sommer, A. & Simon, J. Synthetic Landau levels for photons. *Nature* **534**, 671–675 (2016).
30. Sala, V. et al. Spin-orbit coupling for photons and polaritons in microstructures. *Phys. Rev. X* **5**, 011034 (2015).
31. Qi, X.-L. & Zhang, S.-C. The quantum spin Hall effect and topological insulators. *Phys. Today* **63**, 33 (2010).
32. Fu, L. Topological crystalline insulators. *Phys. Rev. Lett.* **106**, 106802 (2011).
33. Linder, N. H., Refael, G. & Galitski, V. Floquet topological insulator in semiconductor quantum wells. *Nat. Phys.* **7**, 490–495 (2011).
34. Hafezi, M., Mittal, S., Fan, J., Migdall, A. & Taylor, J. M. Imaging topological edge states in silicon photonics. *Nat. Photon.* **7**, 1001–1005 (2013).
35. Khanikaev, A. B. et al. Photonic topological insulators. *Nat. Mater.* **12**, 233–239 (2013).
36. Gao, F. et al. Probing topological protection using a designer surface plasmon structure. *Nat. Commun.* **7**, 11619 (2016).
37. Chen, W.-J. et al. Experimental realization of photonic topological insulator in a uniaxial metacrystal waveguide. *Nat. Commun* **5**, 5782 (2014).
38. Cheng, X. et al. Robust reconfigurable electromagnetic pathways within a photonic topological insulator. *Nat. Mater.* **15**, 542–548 (2016).
39. Lai, K., Ma, T., Bo, X., Anlage, S. & Shvets, G. Experimental realization of a reflections-free compact delay line based on a photonic topological insulator. *Sci. Rep.* **6**, 28453 (2016).
40. Slobozhanyuk, A. P. Experimental demonstration of topological effects in bianisotropic metamaterials. *Sci. Rep.* **6**, 22270 (2016).
41. Xiao, B. et al. Exciting reflectionless unidirectional edge modes in a reciprocal photonic topological insulator medium. *Phys. Rev. B* **94**, 195427 (2016).
42. Ma, T., Khanikaev, A. B., Mousavi, S. H. & Shvets, G. Guiding electromagnetic waves around sharp corners: topologically protected photonic transport in metawaveguides. *Phys. Rev. Lett.* **114**, 127401 (2015).
43. Wu, L.-H. & Hu, X. Scheme for achieving a topological photonic crystal by using dielectric material. *Phys. Rev. Lett.* **114**, 223901 (2015).
44. Jung, J., Zhang, F., Qiao, Z. & MacDonald, A. Valley-Hall kink and edge states in multilayer graphene. *Phys. Rev. B* **84**, 075418 (2011).
45. Mittal, S. et al. Topologically robust transport of photons in a synthetic gauge field. *Phys. Rev. Lett.* **113**, 087403 (2014).
46. Ma, T. & Shvets, G. Scattering-free edge states between heterogeneous photonic topological insulators. *Phys. Rev. B* **95**, 165102 (2017).
47. Zhang, Y. et al. Direct observation of a widely tunable bandgap in bilayer graphene. *Nature* **459**, 820–823 (2009).
48. Ezawa, M. Monolayer topological insulators: silicene, germanene, and stanene. *J. Phys. Soc. Jpn* **84**, 121003 (2015).
49. Gorbachev, R. V. et al. Detecting topological currents in graphene superlattices. *Science* **346**, 448–451 (2014).
50. Chen, X.-D. & Dong, J.-W. Valley-protected backscattering suppression in silicon photonic graphene. Preprint at https://arxiv.org/abs/1602.03352 (2016).
51. Chen, X.-D., Zhao, F.-L., Chen, M. & Dong, J.-W. Valley-contrasting physics in all-dielectric photonic crystals: orbital angular momentum and topological propagation. *Phys. Rev. B* **96**, 020202(R) (2017).
52. Noh, J., Huang, S., Chen, K. & Rechtsman, M. C. Observation of photonic topological valley-Hall edge states. Preprint at https://arxiv.org/abs/1706.00059 (2017).
53. Qiao, Z., Jiang, H., Li, X., Yao, Y. & Niu, Q. Microscopic theory of quantum anomalous Hall effect in graphene. *Phys. Rev. B* **85**, 115439 (2012).
54. Ezawa, M. Topological phase transition and electrically tunable diamagnetism in silicene. *Eur. Phys. J.* **85**, 363 (2012).
55. Yao, W., Yang, S. A. & Niu, Q. Edge states in graphene: from gapped flat-band to gapless chiral modes. *Phys. Rev. Lett.* **102**, 096801 (2009).
56. Zhang, F., MacDonald, A. H. & Mele, E. J. Valley Chern numbers and boundary modes in gapped bilayer graphene. *Proc. Natl Acad. Sci. USA* **110**, 10546–10551 (2013).
57. Qiao, Z., Jung, J., Niu, Q. & MacDonald, A. H. Electronic highways in bilayer graphene. *Nano Lett.* **11**, 3453–3459 (2011).
58. Gao, F. et al. Topologically-protected refraction of robust kink states in valley photonic crystals. Preprint at https://arxiv.org/abs/1706.04731 (2017).
59. Yang, Y. et al. Visualization of unidirectional optical waveguide using topological photonic crystals made of dielectric material. Preprint at https://arxiv.org/abs/1610.07780 (2016).
60. Yves, S. et al. Crystalline metamaterials for topological properties at subwavelength scales. *Nat. Commun.* **8**, 16023 (2017).
61. Gorlach, M. A. et al. Controlling scattering of light through topological transitions in all-dielectric metasurfaces. Preprint at https://arxiv.org/abs/1705.04236 (2017).
62. Kitagawa, T., Berg, E., Rudner, M. & Demler, E. Topological characterization of periodically driven quantum systems. *Phys. Rev. B* **82**, 235114 (2010).
63. Fang, K., Yu, Z. & Fan, S. Photonic Aharonov–Bohm effect based on dynamic modulation. *Phys. Rev. Lett.* **108**, 153901 (2012).
64. Fang, K., Yu, Z. & Fan, S. Realizing effective magnetic field for photons by controlling the phase of dynamic modulation. *Nat. Photon.* **6**, 782–787 (2012).
65. Fang, K., Yu, Z. & Fan, S. Experimental demonstration of a photonic Aharonov–Bohm effect at radio frequencies. *Phys. Rev. B* **87**, 060301(R) (2013).
66. Lira, H., Yu, Z., Fan, S. & Lipson, M. Electrically driven nonreciprocity induced by interband photonic transition on a silicon chip. *Phys. Rev. Lett.* **109**, 033901 (2012).
67. Tzuang, L. D., Fang, K., Nussenzveig, P., Fan, S. & Lipson, M. Non-reciprocal phase shift induced by an effective magnetic flux for light. *Nat. Photon.* **8**, 701–705 (2014).
68. Sounas, D. L., Caloz, C. & Alù, A. Giant non-reciprocity at the subwavelength scale using angular momentum-biased metamaterials. *Nat. Commun.* **4**, 2407 (2014).

69. Estep, N. A., Sounas, D. L., Soric, J. & Alù, A. Magnetic-free non-reciprocity and isolation based on parametrically modulated coupled-resonator loops. *Nat. Phys.* **10**, 923–927 (2014).

70. Rechtsman, M. C. et al. Photonic Floquet topological insulators. *Nature* **496**, 196–200 (2013).

71. Maczewsky, L. J., Zeuner, J. M., Nolte, S. & Szameit, A. Observation of photonic anomalous floquet topological insulators. *Nat. Commun.* **8**, 13756 (2017).

72. Mukherjee, S. et al. Experimental observation of anomalous topological edge modes in a slowly driven photonic lattice. *Nat. Commun.* **8**, 13918 (2017).

73. Rudner, M. S., Lindner, N. H., Berg, E. & Levin, M. Anomalous edge states and the bulk-edge correspondence for periodically driven two-dimensional systems. *Phys. Rev. X* **3**, 031005 (2013).

74. Pasek, M. & Chong, Y. Network models of photonic Floquet topological insulators. *Phys. Rev. B* **89**, 075113 (2014).

75. Hu, W. et al. Measurement of a topological edge invariant in a microwave network. *Phys. Rev. X* **5**, 011012 (2015).

76. Atala, M. et al. Direct measurement of the Zak phase in topological Bloch bands. *Nat. Phys.* **9**, 795–800 (2013).

77. Mittal, S., Ganeshan, S., Fan, J., Vaezi, A. & Hafezi, M. Measurement of topological invariants in a 2D photonic system. *Nat. Photon.* **10**, 180–183 (2016).

78. Xiao, M., Zhang, Z. & Chan, C. Surface impedance and bulk band geometric phases in one-dimensional systems. *Phys. Rev. X* **4**, 021017 (2014).

79. Lu, L., Fu, L., Joannopoulos, J. D. & Soljačić, M. Weyl points and line nodes in gyroid photonic crystals. *Nat. Photon.* **7**, 294–299 (2013).

80. Chen, W.-J., Xiao, M. & Chan, C. T. Photonic crystals possessing multiple Weyl points and the experimental observation of robust surface states. *Nat. Commun.* **7**, 13038 (2016).

81. Slobozhanyuk, A. et al. Three-dimensional all-dielectric photonic topological insulator. *Nat. Photon.* **11**, 130–136 (2017).

82. Ozawa, T., Price, H. M., Goldman, N., Zilberberg, O. & Carusotto, I. Synthetic dimensions in integrated photonics: from optical isolation to four-dimensional quantum Hall physics. *Phys. Rev. A* **93**, 043827 (2016).

83. Zilberberg, O. et al. Photonic topological pumping through the edges of a dynamical four-dimensional quantum Hall system. Preprint at https://arxiv.org/abs/1705.08361 (2017).

84. Verbin, M., Zilberberg, O., Kraus, Y. E., Lahini, Y. & Silberberg, Y. Observation of topological phase transitions in photonic quasicrystals. *Phys. Rev. Lett.* **110**, 076403 (2013).

85. Bandres, M. A., Rechtsman, M. C. & Segev, M. Topological photonic quasicrystals: fractal topological spectrum and protected transport. *Phys. Rev. X* **6**, 011016 (2016).

86. Lin, Q., Xiao, M., Yuan, L. & Fan, S. Photonic Weyl point in a two-dimensional resonator lattice with a synthetic frequency dimension. *Nat. Commun.* **7**, 13731 (2016).

87. Dong, J. W., Chen, X. D., Zhu, H., Wang, Y. & Zhang, X. Valley photonic crystals for control of spin and topology. *Nat. Mater.* **16**, 298–302 (2016).

88. St-Jean, P. et al. Lasing in topological edge states of a 1D lattice. Preprint at https://arxiv.org/abs/1704.07310 (2017).

89. Peano, V., Houde, M., Marquardt, F. & Clerk, A. A. Topological quantum fluctuations and traveling wave amplifiers. *Phys. Rev. X* **6**, 041026 (2016).

90. Peano, V., Brendel, C., Schmidt, M. & Marquardt, F. Topological phases of sound and light. *Phys. Rev. X* **5**, 031011 (2015).

91. Karzig, T., Bardyn, C.-E., Lindner, N. H. & Refael, G. Topological polaritons. *Phys. Rev. X* **5**, 031001 (2015).

92. Nalitov, A. V., Solnyshkov, D. D. & Malpuech, G. Polariton Z topological insulator. *Phys. Rev. Lett.* **114**, 116401 (2015).

93. Milićević, M. et al. Orbital edge states in a photonic honeycomb lattice. *Phys. Rev. Lett.* **118**, 107403 (2017).

94. Umucalılar, R. O. & Carusotto, I. Fractional quantum Hall states of photons in an array of dissipative coupled cavities. *Phys. Rev. Lett.* **108**, 206809 (2012).

95. Carusotto, I. & Ciuti, C. Quantum fluids of light. *Rev. Mod. Phys.* **85**, 299–366 (2013).

96. Hafezi, M., Lukin, M. D. & Taylor, J. M. Non-equilibrium fractional quantum Hall state of light. *New J. Phys.* **15**, 063001 (2013).

97. Hormozi, L., Moller, G. & Simon, S. H. Fractional quantum Hall effect of lattice bosons near commensurate flux. *Phys. Rev. Lett.* **108**, 256809 (2012).

98. Zeuner, J. M. et al. Observation of a topological transition in the bulk of a non-Hermitian system. *Phys. Rev. Lett.* **115**, 040402 (2015).

99. Harari, G. et al. in *Conference on Lasers and Electro-Optics*, OSA Technical Digest paper FM3A.3 (Optical Society of America, 2016).

Competing interests

The authors declare no competing financial interests.

Additional information

Reprints and permissions information is available at www.nature.com/reprints.

Correspondence should be addressed to A.B.K. or G.S.

Publisher's note: Springer Nature remains neutral with regard to jurisdictional claims in published maps and institutional affiliations.